Journal Pre-proofs

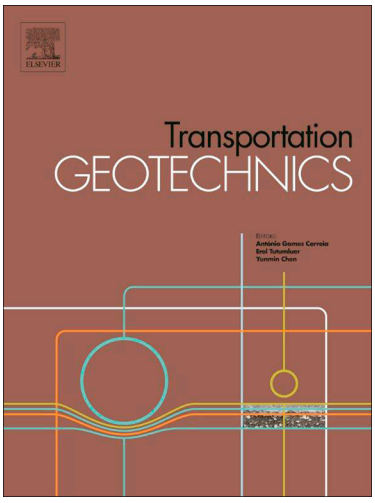

Original Article

Experimental investigation of sandy soil stabilization using chitosan biopolymer

MohammadReza Amiri Tasuji, Pooria Ghadir, Amin Hosseini, Akbar A. Javadi, Asghar Habibnejad Korayem, Navid Ranjbar

PII: S2214-3912(24)00087-4
DOI: https://doi.org/10.1016/j.trgeo.2024.101266
Reference: TRGEO 101266

To appear in: *Transportation Geotechnics*

Received Date: 10 March 2024
Revised Date: 14 April 2024
Accepted Date: 30 April 2024

Please cite this article as: M. Amiri Tasuji, P. Ghadir, A. Hosseini, A.A. Javadi, A. Habibnejad Korayem, N. Ranjbar, Experimental investigation of sandy soil stabilization using chitosan biopolymer, *Transportation Geotechnics* (2024), doi: https://doi.org/10.1016/j.trgeo.2024.101266

Experimental investigation of sandy soil stabilization using chitosan biopolymer

MohammadReza Amiri Tasuji[1], Pooria Ghadir[2,3*], Amin Hosseini[4], Akbar A. Javadi [3], Asghar Habibnejad Korayem[4], Navid Ranjbar[5*]

[1]*Department of Civil Engineering, Iran University of Science and Technology, Tehran, Iran*

[2]*Department of Civil and Environmental Engineering, University of Strathclyde, Glasgow G1 1XJ, United Kingdom*

[3] *Department of Engineering, University of Exeter, Exeter EX4 4QF, United Kingdom*

[4]*Nanomaterials Research Centre, School of Civil Engineering, Iran University of Science and Technology, Tehran 1684613114, Iran*

[5]*Department of Civil and Mechanical Engineering, Technical University of Denmark, 2800 Kgs, Lyngby, Denmark*

[*]*Corresponding authors'* E-mail addresses: Pooria.ghadir@strath.ac.uk (P. Ghadir), naran@dtu.dk (N. Ranjbar)

Graphical Abstract

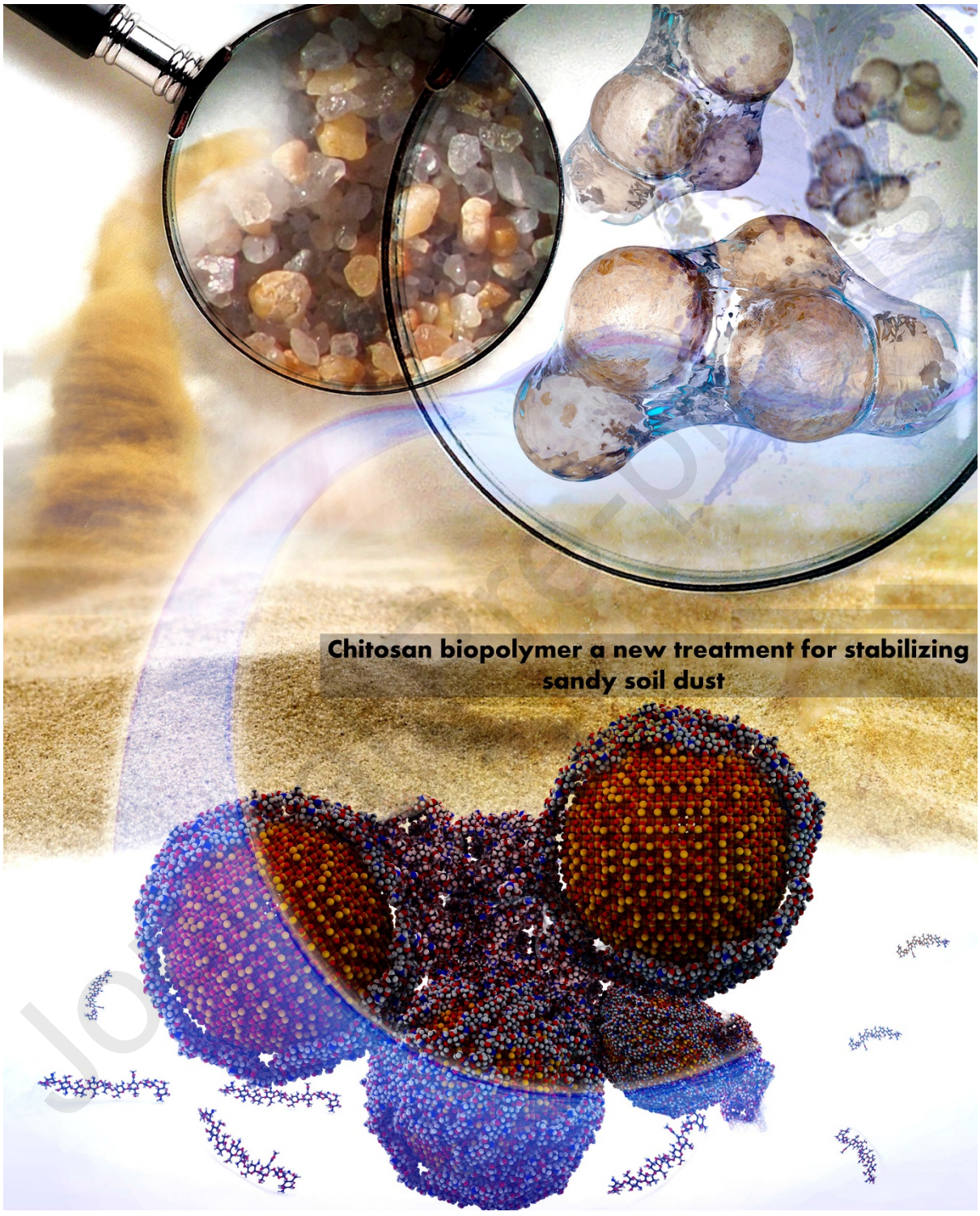

Abstract

The performance of an environmentally friendly biopolymer synthesised from secondary resources to overcome the wind erosion of sandy soil was investigated in this study. The study employed a multi-scale approach to investigate the mechanical, erosional, and hydraulic properties of sandy soil. At the macroscale, experimental techniques such as unconfined and triaxial compression tests, permeability measurements, contact angle assessments, and wind tunnel experiments were utilized to characterize the bulk behavior of the soil. Concurrently, molecular dynamics (MD) simulations were conducted at the nanoscale to predict surface mechanical characteristics and elucidate chemical interactions at the molecular level. Results show that when the outer surface of the sandy particles is coated with a sparse concentration of biopolymer, the sandy aerosol inhibitory performance is significant even under extreme storm conditions reaching speeds of 140 km/h of storms. The study on the impact of biopolymer content, curing time, and curing conditions revealed that the addition of chitosan biopolymer has the ability to enhance the bonding between particles and significantly enhance the mechanical properties of sandy soil. The atomic insight from molecular dynamics reveals huge entanglement between sandy particles and biopolymer by Van der Waals interaction. The results of the Unconfined Compressive Strength test indicate that chitosan enhances the compressive strength of sand by up to 320 kPa. Additionally, the triaxial test demonstrated that the application of chitosan led to a 34.2 kPa improvement in the cohesion of sand. Furthermore, analysis of the permeability test results revealed a decrease in the hydraulic conductivity coefficient from 1.6×10^-6 m/s to 5.7×10^-7 m/s, representing a reduction of approximately 35%.

Keywords: Aerosol; Biopolymer; Sandy soil; Fine dust phenomenon.

1 Introduction

Wind erosion presents a worldwide environmental issue linked to land degradation in dry and semi-dry regions, presenting a serious risk to the ecological environment, sustainable progress, human well-being, and various economic factors. Approximately 5.05×10^6 km^2 of the world's land is degraded by wind erosion, accounting for 46.40 % of the total degraded land area [1]. In principle, wind erosion is a continuous and dynamic process that involves removing soil particles from the ground surface, followed by their movement and deposition [1]. Once the critical lift and drag forces exceed the sum of the gravitational, cohesive, and frictional forces for each soil particle, it begins to roll along the ground surface and then detach from the soil mass and bounce [2]. This process is known as saltation [3]. The amount of soil in motion and its path of transportation rely on factors such as particle size, soil aggregation, and wind velocity. The bounced particles then return with angular momentum, impacting the surface, crushing themselves, and ejecting neighboring particles into wind flow, leading to disaggregation of large particles and emission of finer ones for wind entrainment [3, 4].

In general, the movement of sand-size particles (>0.06 mm [5]) causes the transport trajectories of sand storms to be commonly entrained within the local sources at a relatively close surface to the ground. This process seriously threatens residential, agricultural, and industrial areas [6, 7]. Transportation infrastructure, such as roads and highways, often runs through densely populated areas, exposing people living nearby to higher levels of suspended particles. This pollution impacts infrastructure through corrosion, reduced visibility, and increased maintenance costs. Abu Dhabi

was shrouded in dense dust and sand clouds, which cut the city's vision to 500 meters and caused a 20% rise in the number of asthma sufferers being treated in hospitals [8-10]. On the other side, dust events are those with total suspended particles (TSP) greater than 100 $\mu g/m^3$ particulate matter with aerodynamic diameter below 10 μm (PM_{10}) [11]. Dust can potentially be transferred into the atmosphere as an aerosol is transported thousands of kilometers from source areas by strong winds [10].

There are two major approaches for controlling soil erosion and reducing sand saltation, including chemical binders [12] and mechanical reinforcement (such as plant vegetation or using geosynthetics) [13, 14]. The chemical treatment, such as using oil-based and cementitious materials, is commonly employed to enhance soil erosion resistance by either binding/agglomerating the fine particles together, forming a protective crusted layer, or increasing the surface materials' density against wind entrainment [15]. Different chemical spraying approaches bring different efficiency levels and environment reflections. For example, synthetic polymers, e.g., petroleum mulch, are more durable while having several side effects due to toxicity that potentially causes soil and groundwater contamination and changes soil pH [16]. Similarly, geopolymers are recently used as binders for soil stabilisation; however, their high pH may harm vegetation in the treated area [17-19].

In the past twenty years, there has been significant research into biological methods as alternatives to traditional techniques for stabilizing soil surfaces. [4]. An example of such bio-derived methods is microbial-induced carbonate precipitation (MICP), which triggers the formation of carbonate between soil particles through urease enzyme-catalyzed hydrolysis. [20]. It has already been shown that it is feasible to use the MICP technique and the spraying method to reinforce sands and thus mitigate desertification [21-23]. For example, the erosion rate of treated sand with four MICP treatment cycles was reduced by more than 90% than the untreated sand [24]. Additional hydrolysis processes, like enzyme-induced carbonate precipitation (EICP), utilize urease enzyme obtained from agricultural sources to induce the formation of carbonate among soil particles. [4, 25, 26]. The application of the EICP solution onto the soil surface leads to rapid production of calcium carbonate, facilitated by the presence of free urease enzyme. This enzyme expedites the hydrolysis of urea, especially when a calcium source such as calcium chloride is present. [4]. However, these techniques are significantly environmental dependent (certain temperature and RH) and controlling the growth of binding product is a non-trivial task. For example, in the absence of sufficient oxygen, especially in fine graind soils with compact structure, bacteria are inactive, making the stabilization process inefficient [27].

Biopolymers are another binding material recently used to reduce soil erodibility by enhancing inter-particle cohesion using a relatively small content [28-32]. Biopolymers used in geoscience, such as xanthan gum, carrageenan, chitosan, and cellulose, are mostly polysaccharides; although casein, a protein-based biopolymer, is a naturally renewable resource [33-40]. Several parameters include the chemical and physical properties of soil particles, the structural flexibility of the biopolymers, the quantity of hydroxyl (OH) groups on the surface of both the soil and the biopolymers, and the presence of acid groups (e.g., carboxyl COOH-) in the environment are the dominant determinants of the soil-biopolymer interaction [31, 41, 42].

Chitosan is typically derived from chitin through a process called deacetylation [28, 43]. Chitosan is produced by synthesizing it from different chitin sources, including shrimp and crab [43]. Roughly 1.44 million tons of shell waste from shrimp and crab harvesting is projected annually. Various methods exist for chitosan synthesis. The properties and applications of chitosan are directly impacted by its level of acetylation and molecular weight [43]. Chitosan finds application in environmental scenarios for the purpose of water pollution remediation, targeting substances such as heavy metals, hydrocarbons, and herbicides [44-46]. Moreover, in the realm of geotechnical engineering, chitosan has demonstrated its effectiveness in preventing soil water erosion [47]. The effect of adding chitosan on the mechanical and microstructural characteristics of fine-grained soils was investigated in the previous research [28]; nonetheless, there has been a lack of extensive research into thoroughly examining the interplay between chitosan biopolymer and neutral sand particles. This aspect holds importance since gel-like biopolymers often display limited interaction with cohesionless sand due to the neutral characteristics of the sand particles.

This study encompassed a range of experiments and modeling aimed at examining the function of chitosan biopolymer in the capacity of a binding agent to mitigate sand erosion. The study involved analyses of the mechanical, erosional, and hydraulic characteristics of sandy soil, accomplished through unconfined and triaxial compression tests, alongside assessments of permeability, contact angle, and wind tunnel experiments. On a smaller scale, molecular dynamics (MD) simulations were employed to forecast surface mechanical characteristics and chemical interactions at the nanoscale. MD simulations were additionally utilized to evaluate the interactions between chitosan and the sandy soil matrix, with a primary emphasis on analyzing the stability of atomic structures.

2 Material characterisation and test procedures

2.1 Chitosan hydrogel characteristics

Chitosan is usually extracted from bio-derived wastes following four main stages of demineralisation (decalcification), deproteinisation, dehydration, and deacetylation.

The illustrative diagram depicting the synthesis of chitosan hydrogel is shown in Figure 1a. In this study, a medium molecular weight chitosan biopolymer was obtained from Sigma-Aldrich (CAS number: 9012-76-4). This molecular weight was chosen because increasing chitosan's molecular weight and concentration effectively improve its mechanical properties [48]. The chitosan used in this study had a degree of deacetylation of 82%, therefore, still has the remaining 18% of non-free amino groups in its structure with a high level of viscosity when dissolved in an acetic acid solution, see Figure 1b. In order to create the chitosan solution, chitosan was dissolved in acetic acid at varying percentages of 0.08, 0.16, 0.24, and 0.32 wt.% in relation to the soil's dry weight., see Figure 1c. The appropriate amount of acetic acid required to dissolve chitosan was found through the stepwise addition of 0.01 ml of acetic acid to water, and in each step, the solution was stirred for 5 min, see Figure 1c.

The rheological properties of chitosan solution were measured using an Anton Paar Physica MCR 502 rheometer equipped with a parallel plate system with a 25 mm diameter. The gap was adjusted at 500 μm. All the measurements were carried out at 25 °C using P-PTD200 and H-PTD200 temperature control systems. The measurements were performed in four steps, I) pre-shearing with a constant shear rate of 10 s^{-1} for 30 s; II) 20 s rest; III) increasing shear rate with ramp logarithmic

in the range of 0.01 s^{-1} to 60 s^{-1}; IV) decreasing shear rate with ramp logarithmic in the range of 60 s^{-1} to 0.01 s^{-1}. Step IV was used for analysis in this study. The rheological properties, specifically viscosity, of biopolymer solutions used for preventing soil surface wind erosion play a crucial role in their ability to penetrate and integrate with the target soil. Higher viscosity solutions tend to have limited depth of penetration into the soil structure.

2.2 Soil characteristics

Siliceous sandy soil with uniform grading was obtained from Firoozkuh-Iran. The full particle size was provided in Figure 1d. The remaining physical attributes of this soil, encompassing grain size distribution [49], maximum and minimum soil porosity (e_{max} and e_{min}), specific gravity of soil (Gs) [50], roundness, sphericity, and regularity, are presented in Table 1.

Sand particle roundness, sphericity and regularity show the particle surface morphology and this is an important factor influencing sand structure and mechanical properties. The overall reaction indicates that irregular sand exhibits greater shear strength under lower normal stress compared to round particles. Particle shape has a diminished effect on shear strength under higher normal stress. Irregular sand's shape contributes to a higher proportion of shear bands. Nonetheless, shear band proportion isn't associated with particle sphericity [51]. A Dino-Lite digital microscope (with 200X magnification) was used to take optical images. Optical images of untreated and treated sand are shown in Figures 1e-i and 1e-ii.

Table 1. Sandy soil properties.

Properties	*Gs*	e_{max}	e_{min}	D_{10} *(mm)*	D_{30} *(mm)*	D_{60} *(mm)*	C_u	C_c	*Roundness (R)*	*Sphericity (S)*	*Regularity (ρ)*
Sand	2.658	0.943	0.603	0.2	0.3	0.46	2.58	0.97	*0.6*	*0.79*	*0.70*

Sandy soils are highly susceptible to erosion due to their granular nature and lack of cohesive forces between particles. Consequently, a comprehensive investigation of the mechanical, erosional, and hydraulic properties of sandy soil was deemed necessary to understand and mitigate the erosion susceptibility of such soils. The sand was considered as a representative material for this study because it typifies the characteristics of granular, non-cohesive soils that are prone to erosion by wind and water.

2.3 Mechanical characterisation

2.3.1 Unconfined compressive strength

The uniaxial compressive strength of the materials was measured using an SH-300 hydraulic universal testing machine with a maximum load capacity of 5 kN and precision of 2.5 N on cylindrical samples with dimensions of diameter (D) 38 mm and height (H) 80 mm, based on ASTM D2166 [52]. The loading rate was set to 0.5 mm/min. The quantity of soil utilized for every uniaxial sample was determined by considering the relative density (Dr).[50], as in Equations 1

and 2, which was assumed to be 35% (*Dr* =35%). To maintain consistency in sample compaction, a relative density (Dr) of 35% was targeted for all samples rather than using standard Proctor compaction efforts. This low relative density was selected to replicate the loose state of soil encountered when applying surface additives in wind tunnel testing, where solution is sprayed onto an uncompacted soil surface.

$$Dr = \frac{\left[\frac{1}{\gamma_{d(min)}}\right] - \left[\frac{1}{\gamma_d}\right]}{\left[\frac{1}{\gamma_{d(min)}}\right] - \left[\frac{1}{\gamma_{d(max)}}\right]} \quad (1)$$

$$\gamma_d = \frac{w}{v_s} \quad (2)$$

In Equation 1, γ_d is dry unit weight, $\gamma_{d\ (min)}$ is the minimum dry unit weight, and $\gamma_{d\ (max)}$ is the maximum dry unit weight. In Equation 2, "w" represents the weight of the dry soil, while "v_s" corresponds to the volume of the mold. The specimens were created with a moisture content of 10% by weight in relation to the dry soil weight. The soil was mixed by hand with a chitosan solution for a duration of 5 minutes to ensure a homogenous mixture was prepared[28]. Following this, samples were subjected to three distinct curing conditions: dry condition (DC), moist condition (MC), and submerged condition (SC). The samples were then tested after treatment periods of 7, 14, and 28 days, see Table 2. The compaction of all samples was done in three layers, and each experiment was conducted thrice. Moisture content of the samples was determined by subjecting them to 110°C for 24 hours.

The moisture content of the SC state was about 20%. When preparing the SC samples, the dry soil was first mixed with the chitosan solution, allowing the biopolymer to penetrate and coat the soil particle surfaces as well as partially filling the pore spaces. Upon submergence in water for curing, the chitosan solution already occupying the pore network would have inhibited further moisture infiltration into the sample.

The relative density was consistent at 35% for all test specimens.

Table 2. Summary of the test schedule for the unconfined compression test.

Curing type	Description	Curing time [day]	Concentration of chitosan (wt.%)
DC	Temperature=60 ± 2°C Relative humidity=15 ± 2% Soil moisture content= 0.5 ± 0.1%	7, 14, 28	0.08, 0.16, 0.24, 0.32
MC	Temperature =25 ± 2°C	7, 14, 28	0.08, 0.16, 0.24, 0.32

	Relative humidity=80 ± 2% Soil moisture content= 4 ± 0.5%		
SC	After DC curing, samples were submerged in water for 48 hours Soil moisture content= 20 ± 1%	7, 14, 28	0.08, 0.16, 0.24, 0.32

2.3.2 Triaxial compression test

The contribution of chitosan to soils' particle cohesion and friction was investigated through triaxial compression test. An ELE International equipment in a stress control mode was used. Various concentrations of chitosan including 0.16%, 0.24% and 0.32% were selected for triaxial tests. The dimensions of the mold were diameter (D) 70 mm and height (H) 140 mm. The monotonic consolidated undrained (CU) triaxial tests were performed on both treated and untreated sandy soil based on ASTM D4767 [53]. The CU triaxial test was used since chitosan hydrogel turns the sandy soil specimens into cohesive soils. To perform the triaxial compression, the specimen was first saturated. In order to obtain B value (Skempton) of 0.95 or greater for considering samples as fully saturated, an initial back pressure of 50 kPa under effective stress of 10 kPa, followed by a further increase of about 10 kPa was applied. Then the ratio of changes in pore pressure to stress changes was measured, and B value was calculated. Next, the water was entered into the specimen from a sufficiently elevated tank to gratify the favourite hydraulic gradient. The B value in this study was obtained to be 0.96. The test was operated on the samples cured for 28 days at SC condition.

Tests were performed under three confining pressures of 50, 100, and 150 kPa, and the deformation rate was 0.5 mm/min. The shear strength at a specific confining pressure was calculated using the Mohr-Coulomb criterion as in Equation 3; In this equation, (τ_f) is the shear strength, (c) is interparticle cohesion, (φ) is friction angle, and (σ) is normal stress (confining stress) acting on the failure surface in the form of vertical confinement.

$$\tau_f = c + \sigma \tan(\varphi) \quad (3)$$

2.4 Erosion and hydraulic tests

2.4.1 Wind erosion

A blower-type wind tunnel device was used to characterise specimen's mass loss over wind erosion, see Figures 1f-i and 1f-ii. In principle, a blower-type wind tunnel device directs air into a tunnel by a centrifugal fan and then blows it toward the test section after passing a converging nozzle with an area ratio of 9:1 to a dimension of about 90×90 cm, see Figure 1f-ii. The maximum wind speed in this unit was 144 km/h. The selected wind velocities were 25, 50, 75, 100, 126 and 144 km/h at 5 minutes intervals.

A series of 200 mm×300 mm×70 mm soil specimens with a relative density of 35% (Dr=35%) were prepared for wind tunnel tests. The solution was sprayed on the surface of the specimens with chitosan solution 0.16 and 0.24 wt.%. However, due to the high viscosity of 0.32 wt.% chitosan solution, spraying it on the specimen surface was hardly possible. Thus, this solution was mixed with the soil at a depth of 5 mm from the upper specimen surface. This value was determined because the initial experiment showed that the penetration of the 0.32 wt.% chitosan solution was ~5 mm. The amount of chitosan solution was 0.145 g/cm^2 for all the wind tunnel test specimens. This test was performed on specimens under DC curing condition (after 28 days).

2.4.2 Contact angle

Sessile drop method was used to measure the wettability of biopolymer-treated soils [54]. Samples were prepared in two ways: I) by mixing the soil with chitosan hydrogel II) by coating the specimen surface with chitosan hydrogel. The contact angle was defined based on the angle created between the liquid and the surface of the material.

2.4.3 Permeability

The falling head permeability test was operated according to ASTM D5084 [55] to determine the hydraulic conductivity of biopolymer-treated soils.

The examination was conducted on cylindrical specimens (with a diameter of 70 mm and a height of 140 mm) that were cured under DC conditions for durations of 7 and 28 days. The sample was completely saturated (B value = 0.96), as described in section 2.3.2.

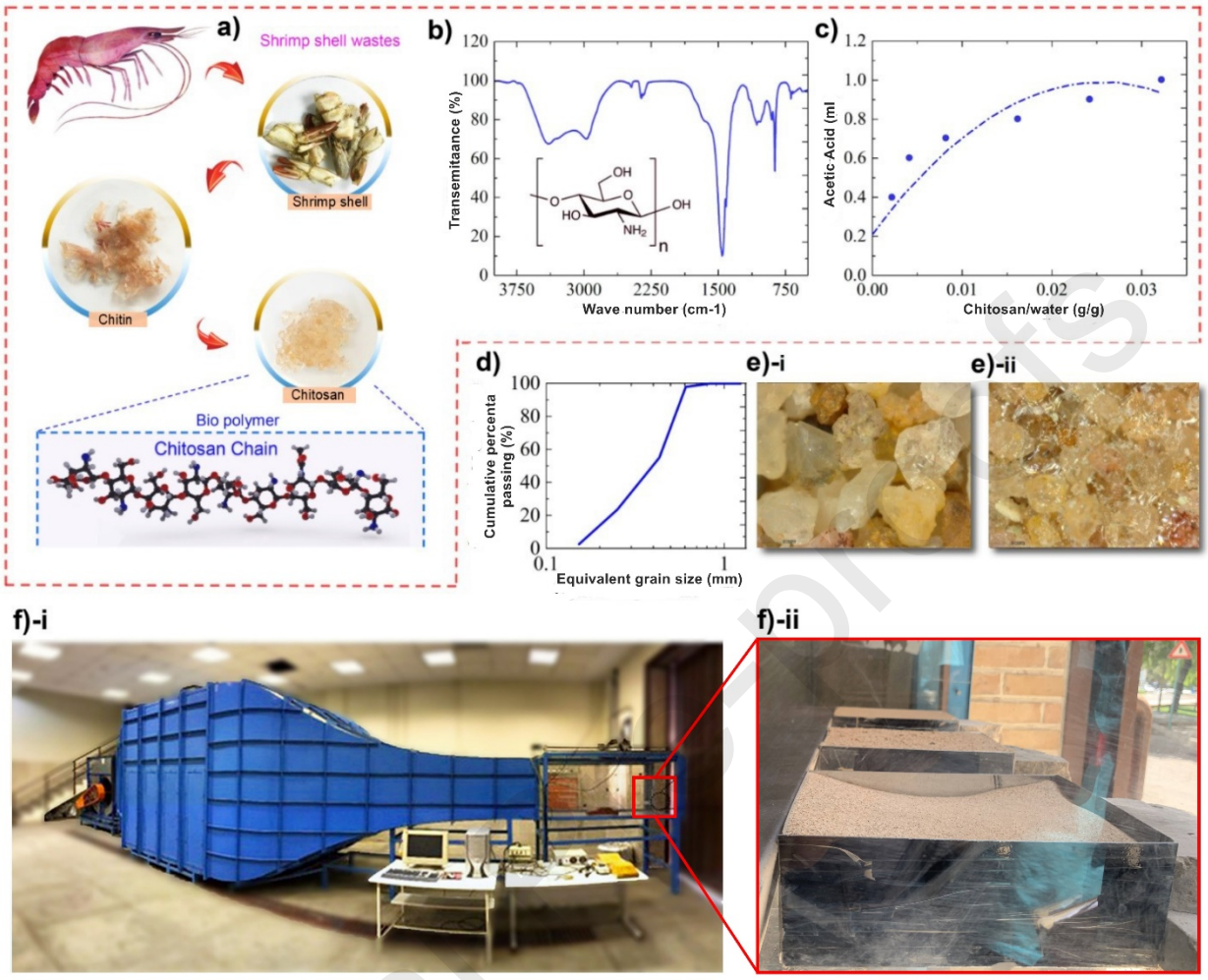

Figure 1. a) Chitosan hydrogel synthesis stages, b) FTIR spectra of the chitosan, c) chitosan solution preparing, d) grain size distribution of base soil, optical images of e)-i pure sand, e)-ii) chitosan-treated sand, f)-i wind tunnel test device, f)-ii wind tunnel test sample.

2.5 Molecular Dynamic (MD) simulations

Molecular dynamics simulations were employed to investigate the adhesion and interaction mechanisms between chitosan and sand particles at the atomic level. Chitosan molecules were confined within a periodic cell with dimensions of 30×30×30 Å (Figure 2a). In contrast, the periodic cells for the silica models, silica-oxygen, and silica-hydroxyl, had dimensions of 30×30×20 Å (Figure 2b-c). In the final setup, chitosan was positioned 3 Å above the silica surface, and any electronic interaction between the two was restricted during this stage. This led to a chitosan-silica cell with dimensions of 30×30×53 Å in the x, y, and z directions, respectively. To accommodate the system appropriately, a vacuum space with a height of 60 Å was added in the Z direction, resulting in a final dimension of 113 Å for the chitosan-silica cell in the z-direction [56].

The COMPASS force field was employed to simulate the interatomic interactions involving chitosan molecules, silica-oxygen, and silica-hydroxyl groups. The system was carefully designed to reach an equilibrium state with the lowest energy level. To achieve this, the SMART method, a combination of the steepest descent, conjugate gradient, and Newton–Raphson methods, was employed to optimize the nanostructures' structure and minimize the energy level [57, 58].

In order to attain dynamic equilibrium, the system underwent analysis for a total duration of up to 1000 ps, within a constant-volume and constant-temperature (NVT) ensemble [59]. The simulation was carried out at 298 K to mimic the surface interaction and reacting process, and a Nose thermostat was used to maintain the temperature at the desired level [60].

Figure 2a provides a visual representation of the atomic structure of chitosan in both its singular molecule and amorphous supercell forms. Meanwhile, Figures 2b and 2c illustrate the silica models, one with oxygen atoms on the surface and the other with hydroxyl groups, capturing the real situations of silica's surface with negative or partial negative charges. Finally, Figures 2d and 2e offer snapshots of the interactions between chitosan and silica-oxygen, as well as silica-hydroxyl, respectively.

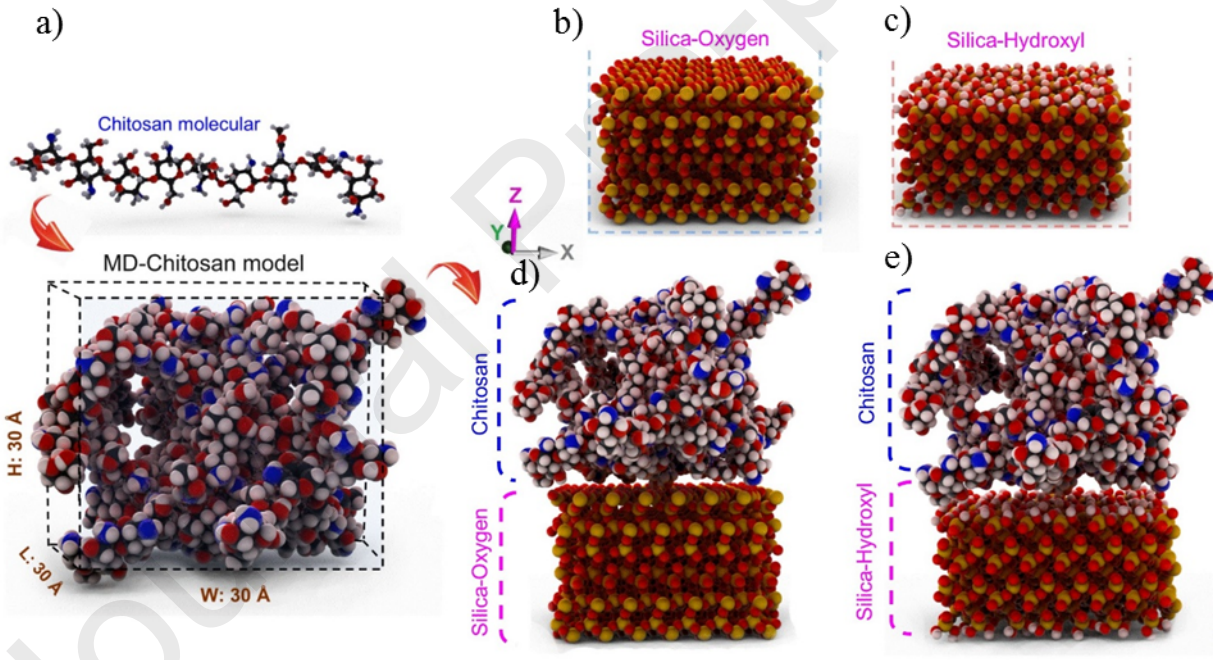

Figure 2. a) The chitosan molecule and the chitosan supercell model, b) the model of silica with oxygen atoms on the surface, c) the model of silica with hydroxyl groups on the surface, d) the model of atomic absorption between silica-oxygen with chitosan on the surface area, and e) the model of atomic absorption between silica-hydroxyl with chitosan on the surface area. The blue, yellow, red, white and grey spheres represent nitrogen, silicon, oxygen, hydrogen, and carbon atoms, respectively.

3 Results and analysis

3.1 Mechanical strength

3.1.1 Unconfined compressive strength

Figure 3 illustrates the uniaxial compressive strength of chitosan-treated sand, with variations observed based on biopolymer content, curing condition, and curing duration. Higher binder content led to increased compressive strength in specimens, but the strength diminished with time in DC and SC conditions, Figures 3a-c. Additionally, compressive strength decreased with increasing moisture levels by comparing DC and SC conditions, Figures 3a-c [29, 32, 61, 62]. Previous research has linked the behavior of chitosan-clay microstructures to the cationic properties of chitosan.

This phenomenon is attributed to the electrical interactions occurring between the biopolymer and the diffuse double layer of clay minerals. This layer encompasses the charged surface and the distributed charge in the surrounding phase. These interactions hold significant importance in governing the behavior of the treated clay particles among themselves [28]. As sand particles lack significant electrical charges, the occurrence of electrostatic and hydrogen bonding phenomena is not to be expected [34]. Hence, the strength of the chitosan-coarse soil mixture predominantly hinges on the potency of the chitosan gel and the ensuing cohesion among particles, a characteristic greatly impacted by the moisture content. The findings show that prolonged exposure to moisture results in a progressive decline in the strength of the sample, indicating a negative correlation between moisture exposure and mechanical integrity. Notably, the impact on strength is more pronounced when the sample is exposed to moisture during the curing process. Conversely, if the sample is initially subjected to drying and subsequently exposed to moisture, the reduction in strength is less severe, as evidenced by the data presented in Figures 3b and 3c. This observation highlights the importance of moisture management during the curing stage and the potential for mitigating strength degradation by implementing appropriate drying protocols prior to moisture exposure.

At DC state, the chitosan hydrogel shrinked due to the dehydration resulting in the formation of dried chitosan fibers that bound the soil grains together, see Figures 3d-f. However, these fibrous connections were brittle and had a small adhesion surface contact with the grains that resulted in brittle failure of the bulk specimen, see Figure 3f. When the material was cured at the elevated moisture level for a long time, the binder retained water in its structure, plasticised, and swelled, see Figure 3f. The hydrogen bonding between the H_2O molecules and chitosan biopolymer due to its hydrophilic surface characteristic caused swelling [28]. “In DC conditions where higher strength is demonstrated, the specimen exhibits lower strains, and as the conditions become wetter, greater strains become observable. This indicates that moisture leads to increased ductility of the soil improved with biopolymer.“ Here, the reduction in unconfined compressive strength with increasing moisture content was attributed to a combination of poor mechanical performance of the binder itself and reduced interlocking forces between the gains covered by the swelled gel. Interestingly, when the DC-cured samples were submerged in water 48 h before the test, the mechanical strength was higher than those cured at ~80% RH for a longer duration. Besides, the moisture content of the SC state was higher than those cured in MC state. This can be explained by the formation of swelled chitosan layer surrounding the specimen that limited further water

penetration to the core. The swelled zone contained a large amount of water and had poor mechanical properties, while the dry core was attributed to the load-bearing capacity. In addition to the influence of moisture, it is known that chitosan is a hydro-degradable material, and over time the adhesive solgel turned into a thick gel that coagulated around the soil grains. Such transformation was the reason for the slight mechanical strength reduction over time.

In other studies on biopolymers, a reduction in strength due to water contact has also been observed. For example, the wetting and drying processes result in a significant decline in the strength and elasticity modulus of both treated and untreated soils. Despite the adverse effects of water soaking on strength, subsequent drying facilitates a considerable restoration of bonding and interactions. Moreover, in wetting and drying conditions, biopolymers significantly contribute to enhancing soil resistance against both strength reduction and mass loss [40, 62].

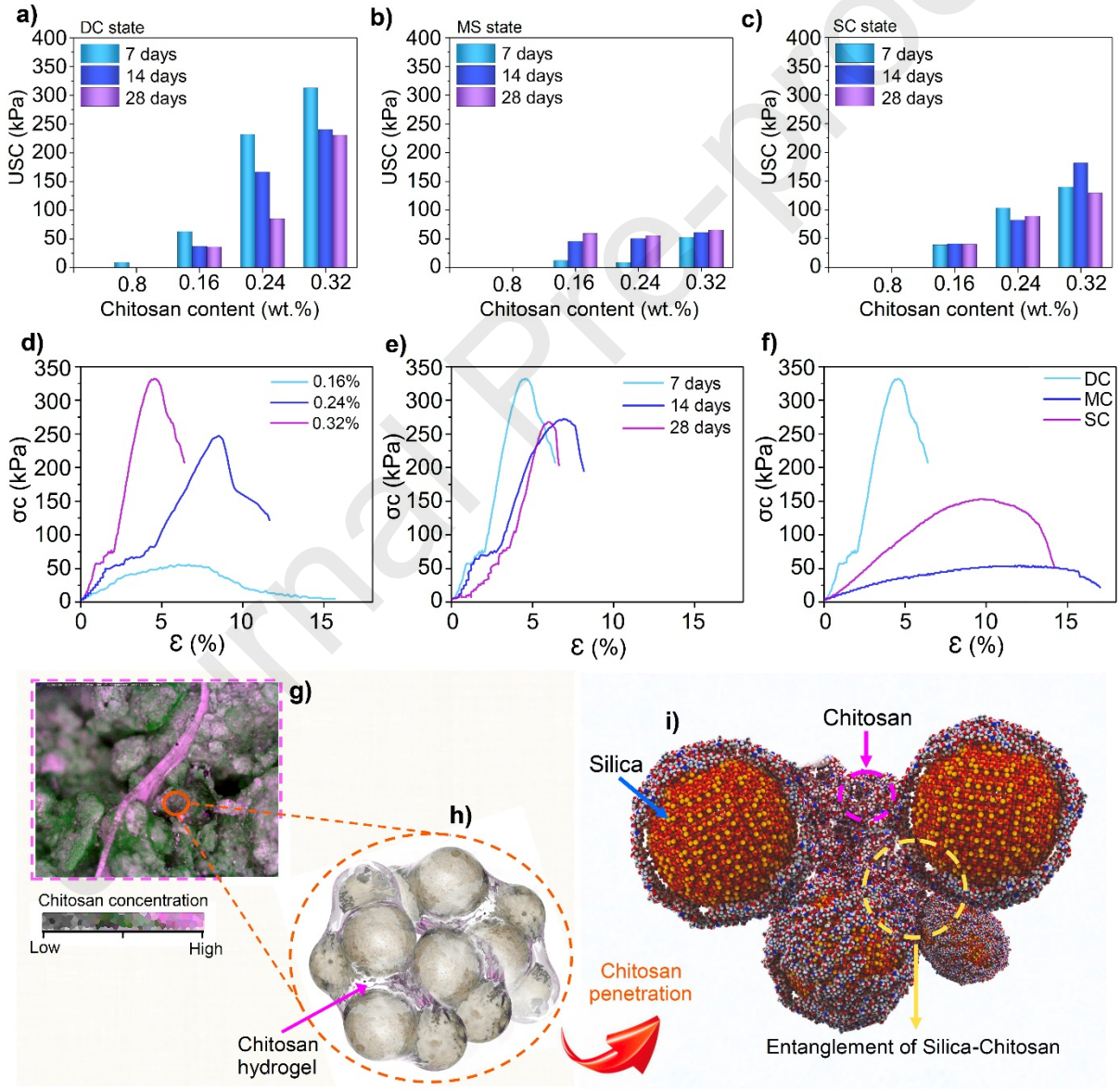

Figure 3. Result of compressive strength tests at a) DC state, b) MC state, c) SC state and stress strain curve at d) 7 days curing (DC state), e) chitosan 0.32 wt.% (DC state), and f) chitosan 0.32 wt.% (7 days curing), g,h) chitosan biopolymer film, i) entanglement silica and chitosan at the atomic scale.

3.1.2 Triaxial compressive strength

Consolidated undrained (CU) tests were performed on the specimens cured at DC under three different confining pressures to get the deviator stress values corresponding to the change in strain, see Table 3. In general, friction angle and confinement are dominant factors of soil strength in cohesionless soils and become more effective when increased. As observed, a higher shear strength was registered for all specimens with higher vertical confinements due to a higher required force to reorient the dense soil structure, intensified with biopolymers' binding contribution. Besides, the shear strength was increased with increased cohesion between the particles using chitosan binder. Figures 3g-i show that in compacted soils, the porosity is less and the concentration of chitosan around the particles increases. Furthermore, an escalation in chitosan concentration led to the progressive filling of pore spaces with chitosan, consequently augmenting the inter-particle distance. This phenomenon facilitated a decreased entanglement between particles, ultimately manifesting in a reduction of the friction angle. Higher shear strength would probably be obtained once the samples became more compact.

The cohesion was amplified by increasing the chitosan concentration, which agrees with the previous studies [32, 61, 63]. However, as expected, the incorporation of chitosan slightly reduced the friction angle of the treated specimens. Indeed, friction angle indicates the interlocking between the soil grains, which depends on various other factors, including particle angularity, soil gradation, and normal stress [32, 63]. In the treated specimens, saturating water plasticises the chitosan polymer network, resulting in a flexible structure surrounding the soil grains. The polymeric network gradually absorbs water and swells until reaching its equilibrium moisture content. This causes a repulsion force between the solid grains and stimulates their internal rearrangement toward reducing the frictional forces and mechanical interlock [64]. The variation in friction angle is expected to be less when the specimen is dried. Figure 4 schematically shows the shear behaviour of untreated and treated sands at different confinement and humidity levels.

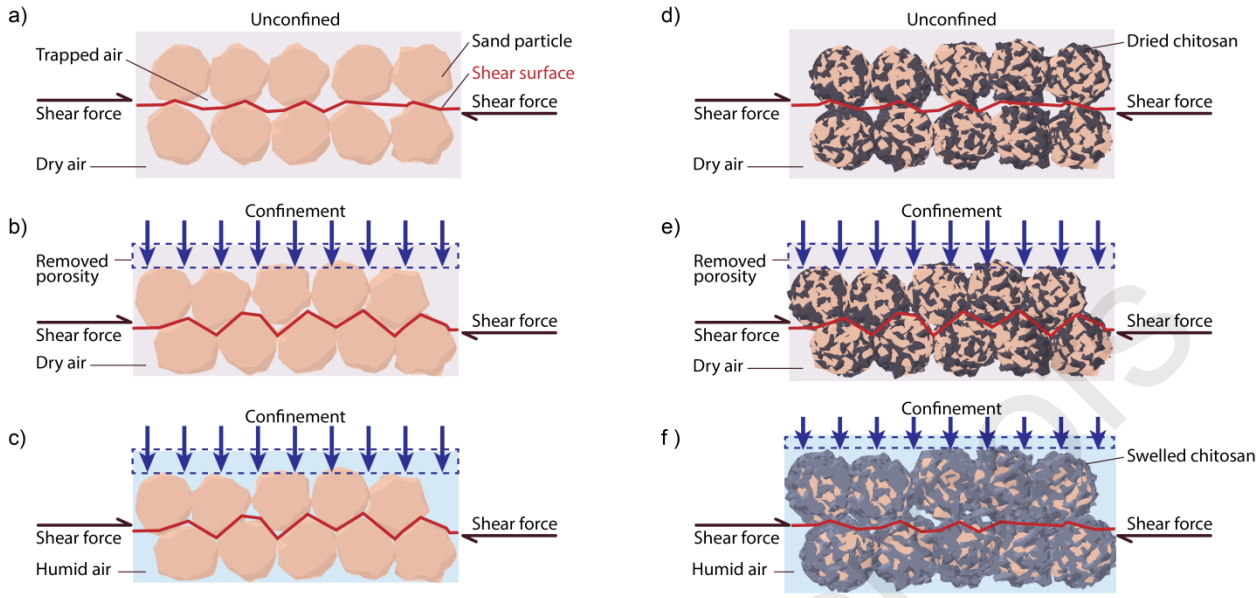

Figure 4. Schematic figure of untreated soil at a) dry/before confinement, b) dry/after confinement, c) wet/after confinement states and treated soil at d) dry/before confinement, e) dry/after confinement, f) wet/after confinement states.

Table 3. Peak deviator stress under different confining pressures (kPa).

	Confining pressure (kPa)					τ (kPa)		
Chitosan content	50	100	150	c (kPa)	φ (degree)	50	100	150
untreated	80.84	160.9	238.4	0.4	26.3	40.4	76.2	108.3
0.16%	118.75	170.21	252.3	24.56	19.2	65.9	87.3	112.4
0.24%	138.51	190.6	243.2	30.2	20.05	80.8	99.8	119.0
0.32%	154.04	208.95	263.8	34.2	20.76	92.6	113.4	134.2

3.2 Molecular Dynamic simulations

We conducted a molecular dynamics simulation to delve into the atomic-scale processes and explore the mechanics of sandy stabilization under dynamic displacements, focusing on interactions between chitosan and silica. Figure 5 illustrates the radial distribution function (RDF) parameters, revealing various atom pairs in chitosan, silica, and chitosan-silica structures.

In the chitosan matrix (Figure 5a), the C−C, C−O, and C−N atom pairs exhibit remarkable prominence. On the contrary, within the silica structure (as depicted in Figure 5b), the Si−O pairs hold prominence, shaping the foundation of the silicate tetrahedral structure and forming the majority of the silica's composition.

Figure 5c highlights a significant peak in the O−H pair when examining the interaction between silica-hydroxyl and chitosan, indicating a strong hydrogen interaction between these species. The H−N pair also plays a crucial role, displaying a notable peak at 2.3 Å. However, due to the lower number of N atoms in chitosan compared to O atoms, their contribution to the overall surface interaction is limited.

On the other hand, in the interaction of silica-oxygen with chitosan, interactions are primarily limited to O atoms of the silica structure with H atoms in chitosan. This leads to repulsion between O and N atoms in chitosan and the silica-oxygen surface, preventing strong interactions with chitosan's H atoms. As a result, there is no specific peak of O-H observed between silica-oxygen and chitosan species in Figure 5c [56].

To comprehensively understand the mechanical behavior at the interface region, we evaluated the interaction between silica and chitosan under shear conditions. We subjected the upper chitosan layer to a 30 Å displacement (Figure 5d) and analyzed the binding energy between the layers (Figure 5e). This energy serves as a gauge of the stability and potency of the van der Waals bonds existing between the silica and chitosan structures.

The outcomes demonstrate that the silica-oxygen and chitosan model exhibit a stronger binding energy compared to the silica-hydroxyl and chitosan model. Specifically, the silica-oxygen and chitosan model display a binding energy 6.4 eV higher than that of the silica-hydroxyl and chitosan model at the initial stage. This distinction persists as the displacement expands, but it vanishes entirely at greater displacements.

The interfacial shear strength values, as shown in Figure 5f, initiate at a high level and progressively decrease during the test due to the reduction in the interacting surface area (anchoring points). Notably, both the silica-hydroxyl and chitosan models consistently demonstrate superior shear strength across the test range. This highlights that incorporating chitosan within the surface region not only bolsters interfacial strength but also augments ductility through heightened shear strength, aligning with the observed increased ductility in tensile testing.

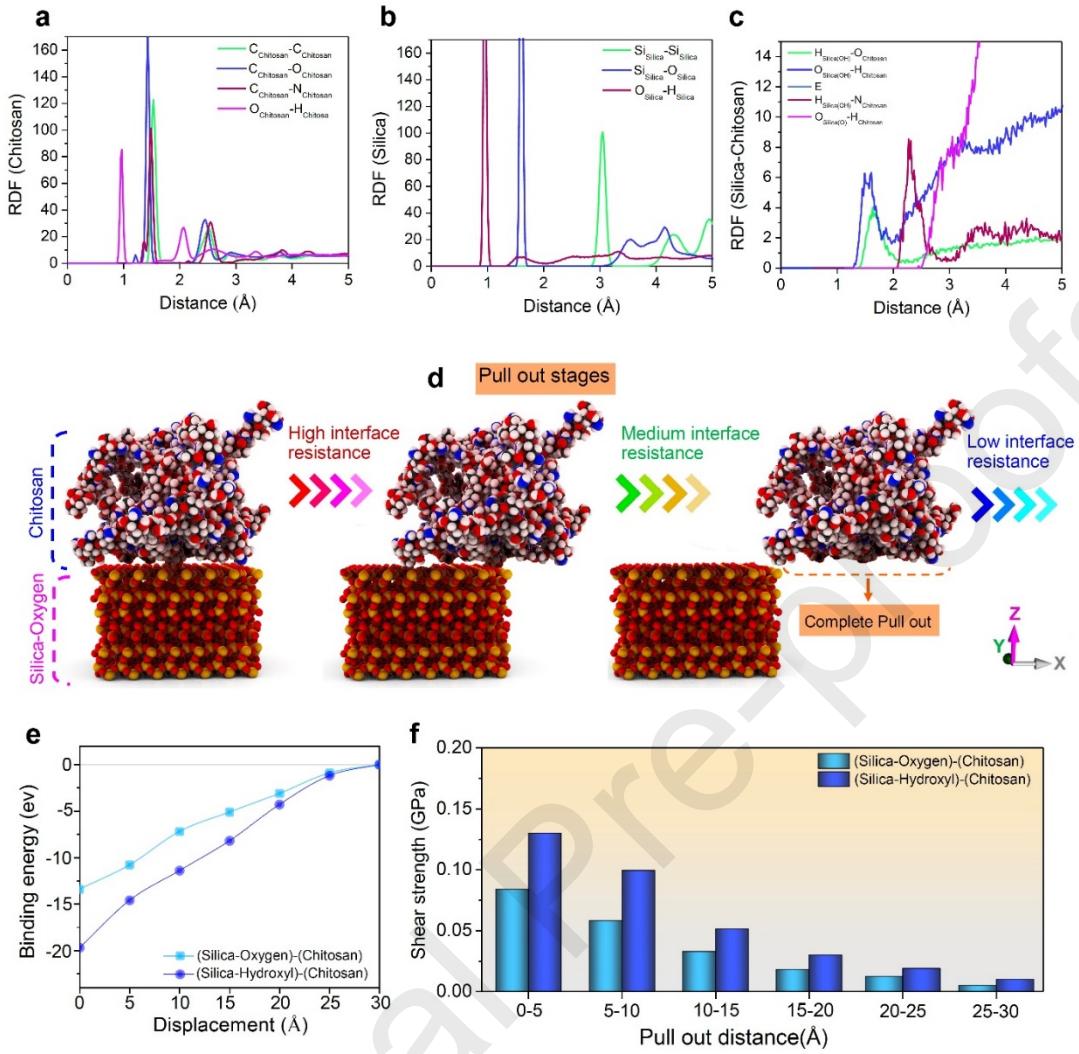

Figure 5. MD analysis, RDF versus distance diagram for a) pristine chitosan molecules, b) pristine silica, and c) atomic pair in the chitosan molecules and silica atoms in the interaction region. Probing of the surficial chitosan is measured using a (d) pull out mechanism with the (e) binding energy and (f) interfacial shear strength used as indices.

3.3 Wind erosion

Figures 6a and 6b show the erosion rate and penetration depth of chitosan-incorporated specimens at various chitosan contents, respectively. The efficiency of chitosan incorporation in enhancing soil erosion resistance was a function of the solution concentration. The biopolymer solution's viscosity significantly affects soil liquid limit. Also, the cohesion parameter is contingent upon the soil's liquid limit and water content [30]. Increasing the viscosity of chitosan solution viscosity increases the liquid limit and shear strength of the soil, which can reduce soil erosion [2]. The reduction in mass loss observed in biopolymer-treated soils can be elucidated by the elevation in undrained shear strength, which arises from the cross-linking of biopolymers between soil particles [2, 30]. On the other hand, Figures 6c and 6d clearly indicate that the shear stress and viscosity of the solution were increased at higher concentrations of chitosan, and thus, limits its transport

through the soil structure, i.e., depth of penetration is reduced at highly concentrated solutions. This influence the levels of integration of soil particles and their response to the wind force. Figure 6e schematically shows soil-biopolymer interaction against wind erosion in untreated and treated soils. Soil particles on the surface under the influence of airflow are affected by erosive and stability forces. Drag, F_d and aerodynamic lift, F_L, are known as erosive and Gravity, F_g, and interparticle cohesion, F_i, are known as stability forces [2].

F_d and F_L remain identical in both scenarios of soil particles, whether with or without disintegration treatment fabric. However, F_g and F_i differ between the two cases. In the case of Figure 6ei, for untreated soil, gravity, F_g is simply the weight of the particles $Fg = mg$, where m is the mass of the particles and g is the acceleration due to gravity and the force of adhesion between the particles, F_i, is present due to shear resistance between soil particles. In the scenario where soil is subjected to treatment with a chitosan solution, the chitosan hydrogel constructs an intricate network among the soil particles. Additionally, it envelops the soil particles present at the surface, a phenomenon visually depicted in Figure 6eii-iii. The application of the biopolymer coating leads to an augmentation in the mass of the soil particles located on the surface, denoted as Fg. Concurrently, the establishment of a cross-linked mesh connecting the soil particles with the biopolymer coating results in the enhancement of the intergranular adhesion force, denoted as Fi. Therefore, the effect of biopolymer on soil erosion not only depends on the increased mechanical strength, but also on the penetration depth to the soil structure.

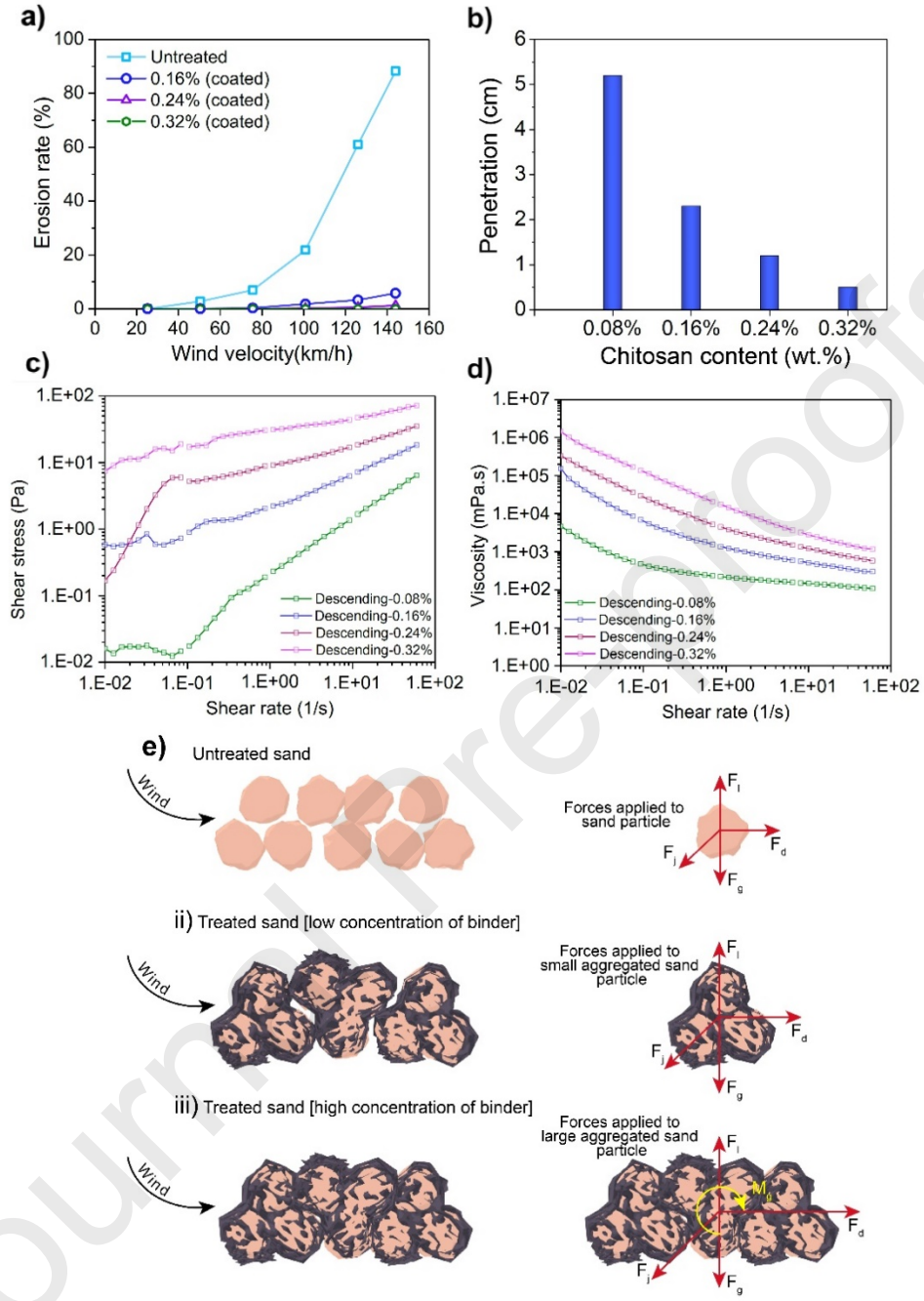

Figure 6. a) wind erosion rate against 25, 50, 75, 100, 126 and 144 km/h wind velocities, b) penetration in different chitosan content, c) shear stress of chitosan solution, d) viscosity of chitosan solution, The soil-biopolymer interaction against wind erosion at ei) untreated soil, eii) treated soil whit low concentration, eiii) treated soil whit high concentration

3.4 Contact angle and permeability assessment

Results in Figure 7a illustrates that chitosan leads to a notable reduction in the permeability of the treated soils, likely through mechanisms such as pore filling or bio-clogging. As an illustration,

the hydraulic conductivity coefficient dropped from 1.6×10^-6 m/s in untreated sandy soil to 5.7×10^-7 m/s in soil treated with 0.32 wt.% chitosan after 28 days curing. Correspondingly, contact angle assessments. (see Figure 7b-d) were performed to measure the degree of wetting when a solid and liquid interact. This test will predict the permeability of soils. This test was carried out on samples with 0, 0.08, 0.16, 0.24 and 0.32 wt.% in mixed and coated specimen types cured in DC state. As observed, all samples coated with 0.08 and 0.16 wt.% kept a drop of water for a short time, and no drops were formed on their surface, so contact angle measurement was impossible. However, water drops remained on the coated sample at an angle of 91° for 0.24 wt.% and 124° for 0.32 wt.%, Figures 7b-d. This is due to the hydrophobic character of the dried chitosan layer, which reduces permeability. Noteworthy, the chitosan layer can absorb water over time if they are in continuous contact. In chitosan mixed samples, due to the large space between the soil particles, the water drop penetrates the samples. Thus, no data was recorded for those specimens. This agrees with the previous observations [29, 31, 47, 65, 66].

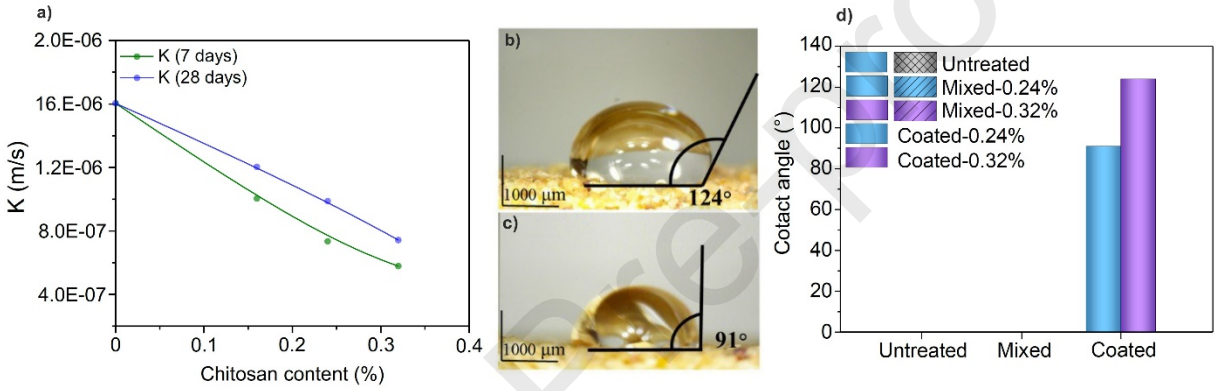

Figure 7. Contact angle test results at a) permeability test results, b) 0.32 wt.% coated specimen, c) 0.24 wt.% coated specimen, and d) untreated, 0.24 wt.% and 0.32 wt.%.

4 Conclusions

This study adopted a multi-scale methodological framework to investigate the mechanical, erosional, and hydraulic characteristics of sandy soil. At the macroscopic scale, a comprehensive array of experimental techniques, including unconfined and triaxial compression tests, permeability measurements, contact angle assessments, and wind tunnel experiments, were employed to characterize the bulk behavior of the sandy soil under various loading and environmental conditions. Concurrently, molecular dynamics (MD) simulations were performed at the nanoscale to predict surface mechanical properties and elucidate the chemical interactions governing the behavior of sandy soil at the molecular level. The findings derived from this study shows that chitosan serves as a potent agent for soil stabilization, demonstrating its efficacy in both the extended duration for sandy soils and the immediate context for clayey soils. This effectiveness arises from the establishment of electrostatic interactions between the chitosan particles and the clay particles. However, such interactions are absent in the case of sand due to its limited surface electrical charge. This allows the biopolymer properties of chitosan in sandy soils to be more stable over time. Soil moisture exerts a predominant influence on the mechanical and

hydraulic characteristics of chitosan-treated soil, with its impact being particularly pronounced on the curing duration. The specimens treated in DC state had the highest strength compared to the MC and SC states. Contact angle and permeability tests have shown that chitosan can reduce the permeability of sand. The higher the chitosan concentration, the lower the sand permeability. When using chitosan to prevent water penetration, it is much more effective to use chitosan as a coating than mixing it with materials. The results of triaxial tests show that chitosan improves soil cohesion but decreases the friction angle, and overall, the shear strength of the soil increases. Wind erosion tests show that chitosan has a positive effect on preventing soil erosion. The foreseen attraction between nucleophile sites on the chitosan (hydroxyl functional group) and the polar sand surface increased adhesion strength. The upward augmentation of energy binding helps to control the aerosol of sandy soil emissions to overcome their intrinsic limitation of weak cohesion, thereby mitigating the key bottleneck of additive industrial in aerosol emissions.

CRediT authorship contribution statement

MohammadReza Amiri Tasuji: Methodology, Formal analysis, Writing - Original Draft. **Pooria Ghadir:** Methodology, Formal analysis, Validation, Writing - Original Draft, Writing - Review & Editing. **Amin Hosseini:** Methodology, Visualization, Writing - Original Draft, Writing - Review & Editing. **Akbar A. Javadi:** Resources, Funding acquisition, Writing – Review & Editing. **Asghar Habibnejad Korayem:** Resources, Writing – Review & Editing. **Navid Ranjbar:** Conceptualization, Supervision, Methodology, Visualization, Funding acquisition, Writing - Review & Editing.

Declaration of competing interest

The authors declare that they have no known competing financial interests or personal relationships that could have appeared to influence the work reported in this paper.

Data availability

Data will be made available on request.

Acknowledgement

Navid Ranjbar would like to acknowledge funding from the research grant (42098) from Villum Fonden. Also, Akbar A. Javadi would like to acknowledge the European Union's Horizon 2020 research and innovation programme under the Marie Sklodowska-Curie, grant number (778120).

Declaration of Generative AI and AI-assisted technologies in the writing process

During the preparation of this work the author(s) used ChatGPT in order to language enhancement. After using this tool/service, the author(s) reviewed and edited the content as needed and take(s) full responsibility for the content of the publication.

References

1. Xu, D. and D. Li, *Variation of wind erosion and its response to ecological programs in northern China in the period 1981–2015.* Land Use Policy, 2020. **99**: p. 104871.

2. Ayeldeen, M., et al., *Laboratory study of using biopolymer to reduce wind erosion.* International Journal of Geotechnical Engineering, 2018. **12**(3): p. 228-240.

3. Chen, R., et al., *Improving dust resistance of mine tailings using green biopolymer.* Environmental Geotechnics, 2019. **8**(6): p. 382-391.

4. Almajed, A., et al., *Mitigating wind erosion of sand using biopolymer-assisted EICP technique.* Soils and Foundations, 2020. **60**(2): p. 356-371.

5. *ASTM D2487-17e1, Standard Practice for Classification of Soils for Engineering Purposes (Unified Soil Classification System)*. ASTM 2017: American Society for Testing and Materials (ASTM), West Conshohocken, PA.

6. Tominaga, Y., T. Okaze, and A. Mochida, *Wind tunnel experiment and CFD analysis of sand erosion/deposition due to wind around an obstacle.* Journal of Wind Engineering and Industrial Aerodynamics, 2018. **182**: p. 262-271.

7. Li, D., et al., *The dynamics of sand-stabilization services in Inner Mongolia, China from 1981 to 2010 and its relationship with climate change and human activities.* Ecological Indicators, 2018. **88**: p. 351-360.

8. Abbasi, H., *Sand Dune Systems in Iran-Distribution and Activity.* 2020.

9. Sprigg, W.A., *Dust storms, human health and a global early warning system.* Extreme Weather, Health, and Communities: Interdisciplinary Engagement Strategies, 2016: p. 59-87.

10. Al-Hemoud, A., et al., *Economic impact and risk assessment of sand and dust storms (SDS) on the oil and gas industry in Kuwait.* Sustainability, 2019. **11**(1): p. 200.

11. Draxler, R.R., et al., *Estimating PM10 air concentrations from dust storms in Iraq, Kuwait and Saudi Arabia.* Atmospheric Environment, 2001. **35**(25): p. 4315-4330.

12. Shariatmadari, N., et al., *Experimental study on the effect of chitosan biopolymer on sandy soil stabilization.* 2020.

13. Guo, J., et al., *Field evaluation of vegetation growth in geocell-reinforced unpaved shoulders.* Geotextiles and Geomembranes, 2015. **43**(5): p. 403-411.

14. Ebrahimi-Khusfi, Z., et al., *Impacts of vegetation anomalies and agricultural drought on wind erosion over Iran from 2000 to 2018.* Applied Geography, 2020. **125**: p. 102330.

15. Preston, C.A., C. McKenna Neuman, and J.W. Boulton, *A wind tunnel and field evaluation of various dust suppressants.* Journal of the Air & Waste Management Association, 2020. **70**(9): p. 915-931.

16. Asadi, P., et al., *Use of modified and petroleum-impregnated bentonite mulch as an eco-friendly stabilizer of wind erodible sands.* Aeolian Research, 2021. **53**: p. 100749.

17. Pu, S., et al., *Environmental behavior and engineering performance of self-developed silico-aluminophosphate geopolymer binder stabilized lead contaminated soil.* Journal of Cleaner Production, 2022. **379**: p. 134808.

18. Ngo, T.-P., et al., *Durability of geopolymer stabilised compacted earth exposed to wetting–drying cycles at different conditions of pH and salt.* Construction and Building Materials, 2022. **329**: p. 127168.

19. Corrêa-Silva, M., et al., *Geomechanical behaviour of a soft soil stabilised with alkali-activated blast-furnace slags.* Journal of Cleaner Production, 2020. **267**: p. 122017.

20. Chang, I., et al., *Review on biopolymer-based soil treatment (BPST) technology in geotechnical engineering practices.* Transportation Geotechnics, 2020. **24**: p. 100385.

21. Mukherjee, S., R.B. Sahu, and J. Mukherjee, *Effect of biologically induced cementation via ureolysis in stabilization of silty soil.* Geomicrobiology Journal, 2022. **39**(1): p. 66-82.

22. Maleki, M., et al., *Performance of microbial-induced carbonate precipitation on wind erosion control of sandy soil.* International journal of environmental science and technology, 2016. **13**: p. 937-944.

23. Dejong, J.T., et al. *Biogeochemical processes and geotechnical applications: progress, opportunities and challenges*. in *Bio-and chemo-mechanical processes in geotechnical engineering: géotechnique symposium in print 2013*. 2014. Ice Publishing.

24. Wang, Z., et al., *Experimental study on wind erosion resistance and strength of sands treated with microbial-induced calcium carbonate precipitation.* Advances in Materials Science and Engineering, 2018. **2018**.

25. Saif, A., et al., *Advances in enzyme induced carbonate precipitation and application to soil improvement: A review.* Materials, 2022. **15**(3): p. 950.

26. He, J., et al., *Enzyme induced carbonate precipitation with fibers for the improvement of clay soil slopes against rainfall and surface runoff erosions.* Transportation Geotechnics, 2023. **42**: p. 101074.

27. Alotaibi, E., et al., *Life cycle assessment of biocemented sands using enzyme induced carbonate precipitation (EICP) for soil stabilization applications.* Scientific Reports, 2022. **12**(1): p. 6032.

28. Hataf, N., P. Ghadir, and N. Ranjbar, *Investigation of soil stabilization using chitosan biopolymer.* Journal of cleaner production, 2018. **170**: p. 1493-1500.

29. Khaleghi, M. and M. Heidarvand, *A novel study on hydro-mechanical characteristics of biopolymer-stabilized dune sand.* Journal of Cleaner Production, 2023. **398**: p. 136518.

30. Mahamaya, M., et al., *Interaction of biopolymer with dispersive geomaterial and its characterization: An eco-friendly approach for erosion control.* Journal of Cleaner Production, 2021. **312**: p. 127778.

31. Lee, M., et al., *Strengthening and permeability control in sand using Cr3+-crosslinked xanthan gum biopolymer treatment.* Transportation Geotechnics, 2023. **43**: p. 101122.

32. Jamshidi, M., et al., *Effect of chitosan bio-polymer stabilization on the mechanical and dynamic characteristics of marl soils.* Transportation Geotechnics, 2023. **42**: p. 101110.

33. Nouri, H., et al., *Effects of Protein-Based Biopolymer on Geotechnical Properties of Salt-Affected Sandy Soil.* Geotechnical and Geological Engineering, 2022. **40**(12): p. 5739-5753.

34. Chang, I., et al., *Effects of Xanthan gum biopolymer on soil strengthening.* Construction and Building Materials, 2015. **74**: p. 65-72.

35. Chang, I., J. Im, and G.-C. Cho, *Introduction of microbial biopolymers in soil treatment for future environmentally-friendly and sustainable geotechnical engineering.* Sustainability, 2016. **8**(3): p. 251.

36. Fatehi, H., et al., *Biopolymers as green binders for soil improvement in geotechnical applications: A review.* Geosciences, 2021. **11**(7): p. 291.

37. Ni, J., Z.-T. Wang, and X. Geng, *Vegetation growth promotion and overall strength improvement using biopolymers in vegetated soils.* Canadian Geotechnical Journal, 2023(ja).

38. Ni, J., S.-S. Li, and X.-Y. Geng, *Mechanical and biodeterioration behaviours of a clayey soil strengthened with combined carrageenan and casein.* Acta Geotechnica, 2022. **17**(12): p. 5411-5427.

39. Ni, J., et al., *Performance of soils enhanced with eco-friendly biopolymers in unconfined compression strength tests and fatigue loading tests.* Construction and Building Materials, 2020. **263**: p. 120039.

40. Fatehi, H., et al., *Sustainable soil treatment: Investigating the efficacy of carrageenan biopolymer on the geotechnical properties of soil.* Construction and Building Materials, 2024. **411**: p. 134627.

41. Martin, J.P., *Decomposition and binding action of polysaccharides in soil.* Soil Biology and Biochemistry, 1971. **3**(1): p. 33-41.

42. Chang, I., et al., *Strength durability of gellan gum biopolymer-treated Korean sand with cyclic wetting and drying.* Construction and Building Materials, 2017. **143**: p. 210-221.

43. Younes, I. and M. Rinaudo, *Chitin and chitosan preparation from marine sources. Structure, properties and applications.* Marine drugs, 2015. **13**(3): p. 1133-1174.

44. Escudero-Oñate, C. and E. Martínez-Francés, *A review of chitosan-based materials for the removal of organic pollution from water and bioaugmentation.* Chitin-Chitosan-Myriad Functionalities in Science and Technology, 2018. **1**.

45. de Moraes, M.A., et al., *Chitosan and alginate biopolymer membranes for remediation of contaminated water with herbicides.* Journal of Environmental Management, 2013. **131**: p. 222-227.

46. Boamah, P.O., et al., *Sorption of heavy metal ions onto carboxylate chitosan derivatives—A mini-review.* Ecotoxicology and Environmental Safety, 2015. **116**: p. 113-120.

47. Aguilar, R., et al., *The potential use of chitosan as a biopolymer additive for enhanced mechanical properties and water resistance of earthen construction.* Construction and Building Materials, 2016. **114**: p. 625-637.

48. Tai, K., et al., *The stabilization and release performances of curcumin-loaded liposomes coated by high and low molecular weight chitosan.* Food Hydrocolloids, 2020. **99**: p. 105355.

49. *ASTM D6913-04, Standard Test Methods for Particle-Size Distribution (Gradation) of Soils Using Sieve Analysis*. ASTM 2009: American Society for Testing and Materials (ASTM), West Conshohocken, PA.

50. *ASTM D4254-00, Standard Test Methods for Minimum Index Density and Unit Weight of Soils and Calculation of Relative Density*. ASTM 2006: American Society for Testing and Materials (ASTM), West Conshohocken, PA.

51. Chen, C., et al., *Discrete element modeling of particles sphericity effect on sand direct shear performance.* Scientific Reports, 2022. **12**(1): p. 5490.

52. *ASTM D2166-16, Standard test method for unconfined compressive strength of cohesive soil*. ASTM 2016: American Society for Testing and Materials (ASTM), West Conshohocken, PA.

53. *ASTM D4767, Standard test method for consolidated undrained triaxial compression test for cohesive soil*. ASTM 2010: American Society for Testing and Materials (ASTM), West Conshohocken, PA.

54. Yuan, Y. and T.R. Lee, *Contact angle and wetting properties*, in *Surface science techniques*. 2013, Springer. p. 3-34.

55. *ASTM D5084, Standard Test Methods for Measurement of Hydraulic Conductivity of Saturated Porous Materials Using a Flexible Wall Permeameter*. ASTM 2016: American Society for Testing and Materials (ASTM), West Conshohocken, PA.

56. Hosseini, E., et al., *Robust cleaning mechanism permanently detaches hydrocarbon species from silicate surfaces by amphiphiles.* Applied Surface Science, 2021. **558**: p. 149954.

57. Bhuvaneshwari, B., et al., *Nano mechanical properties on the mineralogical array of calcium silicate hydrates and calcium hydroxide through molecular dynamics—CSIR–SERC.* Current Science, 2015: p. 1058-1065.

58. Wang, X., et al., *Interfacial binding energy between calcium-silicate-hydrates and epoxy resin: A molecular dynamics study.* Polymers, 2021. **13**(11): p. 1683.

59. Sanchez, F. and L. Zhang, *Molecular dynamics modeling of the interface between surface functionalized graphitic structures and calcium–silicate–hydrate: interaction energies, structure, and dynamics.* Journal of colloid and interface science, 2008. **323**(2): p. 349-358.

60. Kai, M., L. Zhang, and K. Liew, *Graphene and graphene oxide in calcium silicate hydrates: Chemical reactions, mechanical behavior and interfacial sliding.* Carbon, 2019. **146**: p. 181-193.

61. Liu, J., et al., *Performance and mechanism of a novel biopolymer binder for clayey soil stabilization: Mechanical properties and microstructure characteristics.* Transportation Geotechnics, 2023: p. 101044.

62. Fatehi, H., et al., *The effects of particle size distribution and moisture variation on mechanical strength of biopolymer-treated soil.* Polymers, 2023. **15**(6): p. 1549.

63. Smitha, S., K. Rangaswamy, and D. Keerthi, *Triaxial test behaviour of silty sands treated with agar biopolymer.* International Journal of Geotechnical Engineering, 2021. **15**(4): p. 484-495.

64. Pereda, M., M.I. Aranguren, and N.E. Marcovich, *Water vapor absorption and permeability of films based on chitosan and sodium caseinate.* Journal of Applied Polymer Science, 2009. **111**(6): p. 2777-2784.

65. Nakamatsu, J., et al., *Eco-friendly modification of earthen construction with carrageenan: Water durability and mechanical assessment.* Construction and Building Materials, 2017. **139**: p. 193-202.

66. Fertahi, S., et al., *Properties of coated slow-release triple superphosphate (TSP) fertilizers based on lignin and carrageenan formulations.* ACS Sustainable Chemistry & Engineering, 2019. **7**(12): p. 10371-10382.

Graphical Abstract

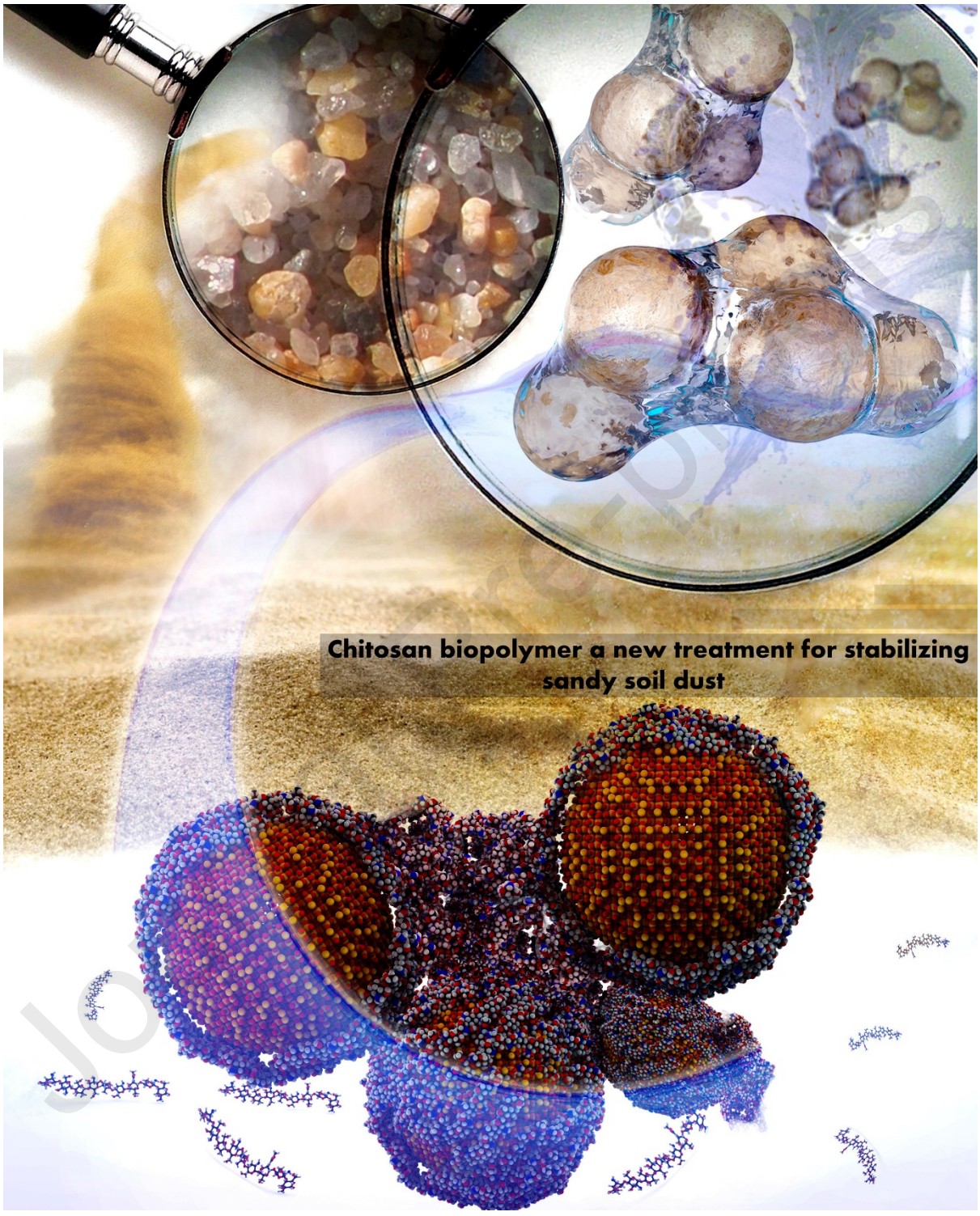

Declaration of competing interest

The authors declare that they have no known competing financial interests or personal relationships that could have appeared to influence the work reported in this paper.